Title

Atmospheric History of H2 Over the Past Century Reconstructed From South Pole Firn Air

Permalink

https://escholarship.org/uc/item/6vk3n2nt

Journal

Geophysical Research Letters, 47(14)

ISSN

0094-8276

Authors

Patterson, JD
Aydin, M
Crotwell, AM
et al.

Publication Date

2020-07-28

DOI

10.1029/2020gl087787

Peer reviewed

Correspondence to:
J. D. Patterson,
jdpatter@uci.edu

Atmospheric History of H_2 Over the Past Century Reconstructed From South Pole Firn Air

J. D. Patterson[1] , M. Aydin[1] , A. M. Crotwell[2,3], G. Petron[2,3], J. P. Severinghaus[4] , and E. S. Saltzman[1]

[1]Departments of Earth System Science and Chemistry, University of California, Irvine, CA, USA, [2]Global Monitoring Division, Earth System Research Laboratory, National Oceanic and Atmospheric Administration, Boulder, CO, USA, [3]Cooperative Institute for Research in Environmental Sciences, University of Colorado, Boulder, CO, USA, [4]Scripps Institution of Oceanography, University of California, San Diego, La Jolla, CA, USA

Abstract Molecular hydrogen (H_2) is an abundant and reactive constituent of Earth's atmosphere, with links to climate and air quality. Anthropogenic emissions of H_2 are expected to rise as the use of H_2 as an energy source increases. Documenting past variations in atmospheric H_2 will help to validate current understanding of the global H_2 budget. The modern instrumental record begins in the 1980s; there is little information about atmospheric H_2 prior to that time. Here, we use firn air measurements from a 2001 South Pole campaign to reconstruct atmospheric H_2 levels over the 20th century. Inversion of the measurements indicates that H_2 over South Pole has increased from 350–540 ppb from 1910–2000. A biogeochemical box model indicates that the atmospheric burden of H_2 increased by 37% over that time. The rise in H_2 is consistent with increasing H_2 emissions from fossil fuel combustion and increasing atmospheric production from methane oxidation.

Plain Language Summary Hydrogen (H_2) is an atmospheric trace gas with both natural and anthropogenic sources. In the atmosphere, photochemical reactions of H_2 can contribute to air pollution and influence climate. Future use of hydrogen as a possible replacement for fossil fuels will likely lead to increased emissions and atmospheric levels. Here we use measurements of hydrogen in South Pole firn air to reconstruct atmospheric hydrogen levels over the 20th century. We find that atmospheric H_2 increased by about 40% over that time. This increase is consistent with estimates of emissions of hydrogen and hydrogen precursors from fossil fuel burning.

1. Introduction

Molecular hydrogen (H_2) is a reactive trace gas with a complex biogeochemical cycle and emissions from both natural and anthropogenic sources. Anthropogenic H_2 emissions will increase significantly in coming decades due to growing use of H_2 as a fuel, but projecting the atmospheric response requires a thorough understanding of the global biogeochemical cycle. Documenting the historical levels of H_2 in the atmosphere is useful in order to understand the natural cycling of this trace gas, to quantify man's impact to date, and to validate models for projecting future trends.

The major sources of H_2 are biomass burning, fossil fuel combustion, and photolysis of carbonyl compounds derived from the photo-oxidation of methane and nonmethane hydrocarbons (NMHCs). The major sinks are microbial uptake in soils and atmospheric oxidation by OH. H_2 has an average atmospheric abundance of about 530 ppb (nmol mol^{-1}) and an atmospheric lifetime of 2 years (Ehhalt & Rohrer, 2009; Novelli et al., 1999; Price et al., 2007). Southern Hemisphere H_2 levels are about 3% greater than those in the Northern Hemisphere due to the N/S hemispheric asymmetry in the soil sink (Novelli et al., 1999).

Tropospheric oxidation of H_2 occurs by reaction with OH and results in net O_3 production and an increase in the lifetime of methane and NMHCs (Novelli et al., 1999; Prather, 2003; Schultz et al., 2003; Wang, Jia, Olsen, Wuebbles, Dubey, & Rockett, 2013). In the stratosphere, H_2 is a precursor of water vapor and HO_2 with direct radiative effects through IR absorption, and indirect radiative effects due to catalytic loss of ozone and changes in the frequency and distribution of polar stratospheric clouds (Tromp et al., 2003; Wang, Jia, Olsen, Wuebbles, Dubey, Rockett, & Wuebbles, 2013).

The instrumental record indicates that atmospheric H_2 has not changed dramatically since the early 1990s (Khalil & Rasmussen, 1990; Novelli et al., 1999). Earlier studies reported a wide range (400–2,000 ppb) but likely reflect analytical issues and/or influence from urban pollutants. (Ehhalt et al., 1977; Paneth, 1937; Schmidt, 1974). A Greenland firn air record indicates atmospheric levels ranging from 400–480 ppb during the 1960s to a maximum of 500–520 ppb from 1980–1995, followed by a recent decline to about 480 ppb in 2010 (Petrenko et al., 2013). As noted by the authors, the firn air modeling in that study did not account for pore close-off fractionation of H_2. It is possible that the inferred late 20th century maximum is an artifact due to that process. The recent decline deduced from the firn air record is inconsistent with the instrumental observations showing high northern latitude H_2 levels of roughly 500 ppb since the mid-1990s (Novelli et al., 1999; NOAA/GMD: ftp://aftp.cmdl.noaa.gov/data/trace_gases/h2/) .

Here we report South Pole firn air H_2 measurements of samples collected during the 2001 field season and analyzed at NOAA/GMD in March 2001 and February 2002 (Severinghaus & Battle, 2006). A firn air model is used to reconstruct Southern Hemisphere atmospheric H_2 levels over the 20th century. The inferred changes in H_2 are examined to assess human impact on the atmospheric H_2 budget.

2. Firn Air Measurements and Reconstructing the Atmospheric History

2.1. Field Sampling, H_2 Analysis, and Data Processing

South Pole firn air samples were taken at the surface and at 27 unique depths. Firn air samples were dried using a P_2O_5 desiccant and stored in 2L NOAA/CCGG glass flasks sealed with Louwers-Hapert valves with Viton o-rings. Replicate samples were collected at selected depths. In total, 111 flask measurements for H_2 were made. Of these, 15 measurements were rejected due to documented analytical problems (supporting information). The remaining 96 measurements are plotted in Figure 1a. The firn air samples were analyzed for H_2 at NOAA/GMD by gas chromatography with a mercuric oxide reductive gas analyzer (HgO-RGA). The relative measurement precision is estimated to be $\pm 2\%$. The data are corrected for the nonlinear response of the HgO-RGA. The data are also corrected for the offset between the NOAA96 calibration scale and the current World Meteorological Organization recommended Max Plank Institute 2009 calibration scale (MPI2009). Measurements are reported as dry air mole fractions (ppb = nmol mol^{-1}; Novelli et al., 1999). Details about these corrections are provided in the supporting information.

H_2 measurements from 0–116 m were corrected for gravitational fractionation using the barometric equation (1.7% at 116 m; Bender et al., 1994; Craig et al., 1988). $\delta^{15}N_2$ was constant from 116–123 m, indicating the onset of the lock-in zone, a region characterized by seasonal alternation of permeable and impermeable layers. The barometric correction for 116 m was applied throughout the lock-in zone. Samples from the top 35 m were not used because of the influence of seasonal variations in composition of the overlying atmosphere (Aydin et al., 2011). The 121.6 m sample was also rejected as an outlier (supporting information).

The depth-averaged firn air measurements show a roughly linear increase from about 400 ppb H_2 at 122.9 m to near modern levels at 114.8 m. Above 114.8 m, H_2 is roughly constant near 540 ppb. Uncertainties are the standard deviation (σ) of measurements from the same depth including the propagated analytical uncertainty (Figure 1b). For depths at which there is only one measurement, the largest σ from all depths is used.

2.2. Firn Air Modeling

A one-dimensional finite difference advective/diffusive firn air model was coded in MATLAB (Mathworks, Inc.) and used to simulate H_2 in South Pole firn air. We refer to this new model as UCI_2 to distinguish from previous UCI firn air models. The model grid, integration scheme, and most of the parameterization of gas advection/diffusion are based on Severinghaus and Battle (2006; hereafter SB2006). The principle differences between UCI_2 and SB2006 are as follows: (1) UCI_2 is formulated in terms of concentration of trace gas (mol m^{-3}) rather than enrichment, and (2) UCI_2 has the option to use either equilibrium or kinetic parameterizations for pore close-off fractionation.

Firn physical properties in the model are from SB2006. The average annual temperature is $-51°C$, and the annual accumulation rate is 8 cm year^{-1} ice equivalent. The bulk density of the firn in each grid layer is prescribed from an empirical fit to density measurements on the firn core. The total porosity (s) is calculated from the bulk firn density:
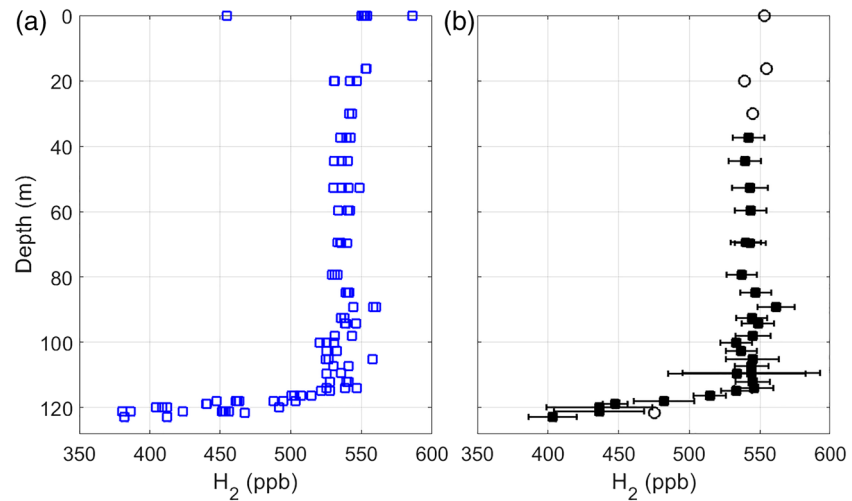
Figure 1. Depth profiles of (a) measurements of H_2 from the South Pole 2001 firn sampling expedition corrected for the nonlinear detector response and calibration scale offset and (b) mean H_2 level at each depth after correcting for gravitational fractionation. Data points excluded from the remainder of this analysis are shown as open circles. Error bars are $\pm 1\sigma$ for measurements at unique depths.

$$s = 1 - \frac{\rho_{\text{firn}}}{\rho_{\text{ice}}}, \tag{1}$$

where ρ_{ice} is the temperature dependent density of ice from Bader (1964; kg m^{-3}). Porosity is partitioned between open firn channels and closed bubbles using an empirical fit between density and closed porosity from Summit, Greenland (Schwander et al., 1993; SB2006). The gas phase diffusivity profile was tuned using the known atmospheric history of CO_2 and the measured depth profile of CO_2. The gas phase diffusivity profile of other gases is determined using the ratio of the gas phase diffusivity of the modeled gas to that of CO_2.

In addition to advective and diffusive transport through open pores, gases with kinetic diameters less than 3.6 Å can permeate through the ice lattice at nonnegligible rates (Ikeda-Fukazawa et al., 2005). Pore close-off fractionation for such gases is important in the lock-in zone, due to permeation from pressurized bubbles to unpressurized open pores. ^{22}Ne enrichments of up to 90‰ were measured in the South Pole 2001 firn air samples and attributed to this process (SB2006). H_2 is also expected to exhibit close-off fractionation because it has a kinetic diameter of 2.89 Å (similar to Ne at 2.75 Å). Here we use two different model approaches (kinetic and equilibrium) to simulate the pore close-off fractionation of H_2 in South Pole firn air.

The kinetic parameterization of close-off fractionation calculates the instantaneous permeation flux of gas n from a single bubble as

$$J_n = \frac{D_n X_n x_n P_{firn} A}{\gamma}, \tag{2}$$

where $D_n X_n$ is the permeation constant of gas n in ice (the product of diffusivity, D_n; [m^2 s^{-1}] and solubility, X_n [mol m^{-3} Pa^{-1}]), x_n is the mole fraction of gas n in the bubble when it closes off, P_{firn} is ambient pressure in the open porosity at bubble close-off (Pa), and A and γ are tunable constants (see SB2006). A is the effective diffusive area (m^2), and γ is a length scale related to bubble geometry, pore geometry, and bubble wall thickness (m). The permeation flux from a given bubble is assumed to be constant from the time of close-off until the bubble has compressed by 5%, after which permeation is assumed to be zero. This parameterization yields good agreement with the measured depth profile of O_2/N_2 using $A/\gamma = 10^{-4}$ m and O_2/N_2 permeation constants given by Ikeda-Fukazawa et al. (2005). The kinetic parameterization also reproduces the enrichment of ^{22}Ne in the South Pole lock-in zone using the same A/γ, if the permeation constant of ^{22}Ne is empirically tuned to 23 times that of O_2 (SB2006).

The permeation constant of H_2 in ice has not been experimentally determined, but it is expected to be larger than that of Ne due to its small diameter and high solubility in ice (Ildyakov & Manakov, 2014). Based on

data from Ildyakov and Manakov (2014) and Satoh et al. (1996), it is possible that permeation is sufficiently rapid that the partial pressure of H_2 would equilibrate fully between the closed bubbles and open pores. The equilibrium parameterization in the UCI_2 model simulates close-off fractionation by imposing equilibrium while maintaining mass balance, as follows:

$$P_n = \left(P_{\text{bubble}}x_{nbubble}s_c + P_{firn}x_{nfirn}s_o\right)/s_{\text{total}},$$ (3)

$$x_{nbubble} = \frac{P_n}{P_{\text{bubble}}},$$ (4)

$$x_{nfirn} = \frac{P_n}{P_{\text{ambient}}},$$ (5)

where P_n is the equilibrium partial pressure of gas n (Pa), x_n is the mole fraction of gas n, P is total gas pressure (Pa), and s_c, s_o, and s_{total} are the dimensionless closed, open, and total porosities, respectively. The subscripts *bubble* and *firn* refer to the closed pores and open pores, respectively. Equations 3–5 are hereafter referred to as the equilibrium parameterization. In both parameterizations, permeation occurs only between closed and open porosity, and all H_2 is assumed to be in either the open or closed pores. Vertical diffusion of H_2 through the ice lattice was neglected. Possible biases resulting from this assumption are small (see the supporting information).

The South Pole firn air H_2 data were analyzed using the UCI_2 model with both the kinetic and equilibrium parameterizations. In the kinetic model runs, we use the permeation constant of ^{22}Ne from SB2006 to represent the lower bound of pore close-off fractions for H_2. The equilibrium parameterization represents the upper bound. Comparing results from the two parameterizations provides an estimate of the sensitivity of the inferred atmospheric H_2 history to assumptions about this process.

2.3. Inversion Methods

The firn air model simulations are initialized with an H_2-free firn air column. A 1-year-long pulse of H_2 is introduced at the surface at the start of the run, and the model is integrated for 300 years using the annual average temperature and accumulation rate for the South Pole (−51°C; 0.08 m ice equivalent per year). The pulse propagates through the firn column, and the H_2 mixing ratio at each depth is recorded as a function of time. This generates a two-dimensional set of age distributions (or Green's functions, $G(z, t)$). The Green's functions provide a computationally efficient means of simulating the South Pole firn air profile ($H_2(z)_{model}$), resulting from a given atmospheric H_2 history ($H_2(t)$), as follows:

$$H_2(z)_{model} = \sum_{t=0}^{300} H_2(t) * G(z, t),$$ (6)

Atmospheric histories reproducing the measured firn air depth profiles were obtained by optimizing the fit between the modeled and measured depth profiles. The MATLAB function, *fmincon*, which employs an interior-point optimization algorithm, is used to minimize a cost function (f). The cost function is defined as the sum of the reduced chi-square statistic $\left(\chi^2_{red}\right)$ and a smoothing term (S). The smoothing term is required for this underconstrained problem to avoid unrealistic high-frequency variations in the reconstructed atmospheric history.

$$f = \chi^2_{\text{red}} + S = \sum_{i=1}^{n} \frac{\left(\frac{\left(H_2(z)_{\text{model}} - H_2(z)_{obs}\right)^2}{\sigma^2}\right)}{n-1} + \alpha \sum_{t=0}^{300} \left(\frac{\partial^2 H_2(t)}{\partial t^2}\right)^2,$$ (7)

where $H_2(z)_{obs}$ is the measured H_2 depth profile, σ is the analytical uncertainty (Figure 1b), n is the number of unique depths in the firn air profile (21), and α is an arbitrary weighting factor for smoothing. Each atmospheric history consists of annual average H_2 mole fractions for the years 1878–2000.

The initial condition for the optimization consists of constant "early industrial" baseline from 1701–1878, followed by a linear increase from 1878–2000, ending at 540 ppb. During the inversion process, H_2 during the baseline period is held constant, and no constraints are placed on the H_2 levels for 1879–2000. A number of tests were conducted to examine the sensitivity of the inversion results to the following parameters:
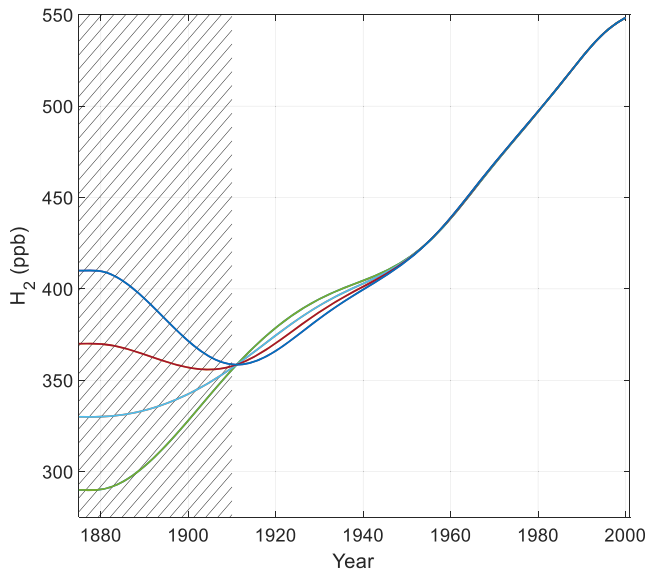
Figure 2. Atmospheric histories of H_2 showing sensitivity of model inversions to the atmospheric H_2 level assumed prior to 1878 at the start of the run. All the runs used $\alpha = .03$ and equilibrium pore close-off fractionation. Four different initial conditions with constant H_2 for baseline preindustrial years were used (290, 330, 370, and 410 ppb), and each line is the average of 1,000 Monte Carlo runs. The results show that the calculated history is sensitive to initial conditions prior to 1910, but relatively insensitive thereafter. From 1910 to 2000, H_2 increased from 357 to 548 ppb.

1. Initial conditions: The baseline atmospheric history (1701–1878) was initialized at four arbitrarily selected levels (290, 330, 370, and 410 ppb).
2. Smoothing: The inversion was run using both, $\alpha = 0.003$ and $\alpha = 0.03$.
3. Measurement uncertainty: a Monte Carlo method was used, in which the sampling and measurement uncertainties at each depth are assumed to be normally distributed. Synthetic firn air profiles are generated by random samples from these distributions.
4. Pore close-off fractionation parameterization: the model was run in both kinetic and equilibrium modes

We emphasize that this technique only quantifies uncertainty in these specific parameters. Bias or uncertainty due to the model physics or ice physical properties is discussed in the supporting information. There are 16 possible combinations of initial conditions, α, and pore-close off fractionation parameterization. A total of 1,000 Monte Carlo runs were performed using each possible combination for a total of 16,000 inversion runs. The baseline tests demonstrated that H_2 atmospheric histories are sensitive to the assumed atmospheric H_2 level prior to 1910 (Figure 2). In subsequent sections, only model results after 1910 are discussed.

3. The Atmospheric History of H_2: Firn Air Model Inversion Results

The ensemble average from reconstructions with $\alpha = .03$, using the equilibrium parameterization yields an H_2 atmospheric history with the following characteristics (Figure 3a). Atmospheric H_2 over the South Pole in 1910 was 357 ± 14 ppb (1σ). After 1910, H_2 increased by 1.5 ppb year^{-1} until 1952. The rate of increase then rose to 2.7 ppb year^{-1} until 2000 when atmospheric levels were 548 ppb. The doubling of the growth rate of
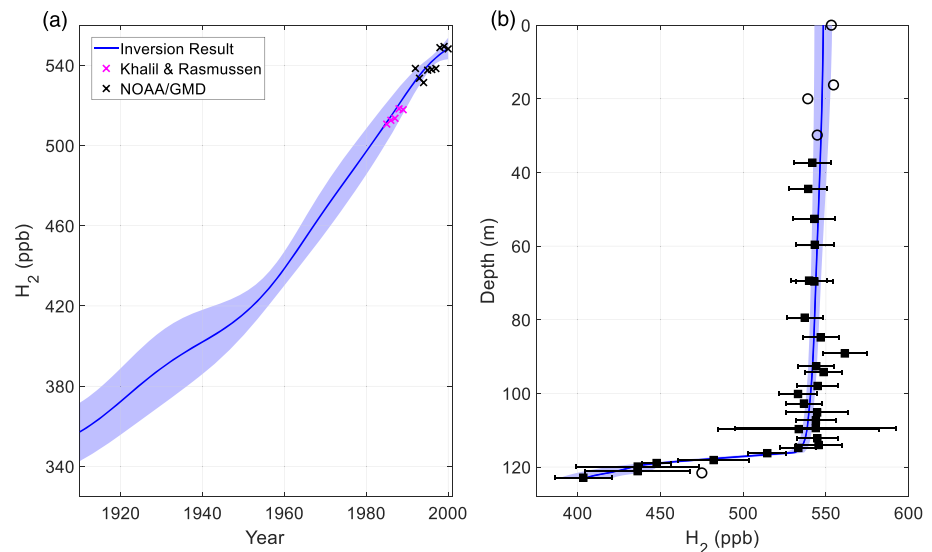

Figure 3. Twentieth century atmospheric history of H_2 inferred from South Pole firn air: (a) blue line and blue shading—mean atmospheric history and $\pm 1\sigma$ uncertainty from 4,000 Monte-Carlo runs (see text). Magenta and black x's—atmospheric H_2 annual means from high southern latitude sites from 1985–1989 and 1992–2000 (Khalil & Rasmussen, 1990; Novelli et al., 1999; NOAA/GMD flask air network). (b) Blue line and shading—mean South Pole firn air H_2 depth profile and $\pm 1\sigma$ uncertainty resulting from the atmospheric history in (a). Firn air H_2 measurements included in the inversion are plotted as black squares with $\pm 1\sigma$ error bars. Measurements excluded from the inversion are plotted as open circles.

Table 1

Sources, sinks, and steady state atmospheric H_2 levels from a biogeochemical box model for the years 1910 and 2000

	1910	2000
Sources (Tg/year)		
Anthro. H_2	1.7 ± 0.4	17.0 ± 4.0
Anthro. NMHC oxidation	0.3 ± 0.3	1.7 ± 1.7
Biog. NMHC oxidation	11.8 ± 6.5	11.8 ± 6.5
Biomass burning	15.0 ± 6.0	15.0 ± 6.0
Methane oxidation	12.1 ± 4.1	23.8 ± 8.0
N_2 fixation—terrestrial	1.6 ± 1.1	3.0 ± 2.0
N_2 fixation—oceans	5.6 ± 3.0	5.0 ± 3.0
Total Sources	48.0 ± 10.4	77.3 ± 13.2
Losses (Tg/year)		
OH oxidation	$13.2 (\pm2.7)$	$21.2 (\pm3.5)$
Soil microbial respiration	$33.5 (\pm6.8)$	$54.8 (\pm9.0)$
Stratospheric loss	$0.8 (\pm0.2)$	$1.3 (\pm.2)$
Total sinks	$48.0 (\pm10.4)$	$77.3 (\pm13.2)$
Box model output		
Tropospheric burden (Tg)	96 ± 20	153 ± 26
South Pole H_2 (ppb)	353 ± 76	545 ± 97
North Pole H_2 (ppb)	290 ± 61	491 ± 81
Interpolar difference (ppb)	63 ± 16	55 ± 21
South Pole firn air model inversion H_2 (ppb)	357 ± 14	548 ± 6

Note. Details regarding source/loss terms and their associated uncertainties are given in the supporting information. The results are a summary of 1,000 Monte Carlo simulations to capture sensitivity to uncertainties in the sources. The result from the firn air inversion is included for comparison.

atmospheric H_2 in the latter half of the 20th century is coincident with a similar increase in the growth rate of atmospheric methane (Etheridge et al., 1998). Methane is the largest source of H_2 in the modern budget.

The major features of the atmospheric reconstructions are insensitive to the choice of pore close-off fractionation parameterization. Kinetic and equilibrium modes produce nearly identical atmospheric histories (supporting information). Some higher-frequency variations in atmospheric H_2 levels are observed using $\alpha = .003$ instead of $\alpha = .03$, but these features should not be considered robust until they are confirmed by additional firn air measurements or ice core measurements (supporting information). For simplicity, the remainder of this discussion will refer to the runs performed under equilibrium mode with $\alpha = .03$.

The firn air-derived H_2 atmospheric history is consistent with the available flask air measurements from high southern latitudes. Those data consist of measurements from 1985–1989 at Palmer Station, Antarctica, and Cape Grim Observatory, Tasmania (Khalil & Rasmussen, 1990) and from 1992–2000 at Palmer, Syowa, South Pole, and Halley stations, Antarctica and Cape Grim Observatory, Tasmania (Novelli et al., 1999; NOAA Global Cooperative Air Sampling Network: ftp://aftp.cmdl.noaa.gov/data/trace_gases/h2/). The maximum deviation of the inversion result from the flask measurements is 1.1% in 1992, and the average deviation is .2% (Figure 3a). NOAA/GMD flask measurements were corrected from the NOAA96 to the MPI2009 calibration scale (supporting information). We have no information about the calibration scale used by Khalil and Rasmussen, so those measurements are not adjusted. The inversions were not constrained by the flask air data.

4. Biogeochemical Modeling: Implications for Changes in the H_2 Budget Over the Past Century

A steady-state tropospheric box model of the H_2 budget was used to compare the firn air-derived atmospheric history to current estimates of the H_2 budget. The model consists of six 30°-wide zonal boxes, with transport based on the modern atmospheric distribution of SF_6 (Marik, 1998). The model includes first-order losses of H_2 to soils, photochemistry, oceans, and the stratosphere. The 2000 budget is based largely on Pieterse et al. (2011), with global emissions of about 78 Tg/year H_2 (Table 1). Simulations are discussed for the years 2000 and 1910.

A minor difference between this and previous models is the inclusion of a dynamic treatment of the oceans. Because the oceans are both a source and sink of H_2, each atmospheric box is coupled to an underlying surface ocean box. The ocean box has a constant oceanic production rate and first-order losses within the water column to simulate microbial cycling and downward advection (Butler, 1994; supporting information). The oceanic source was based on a total ocean H_2 production of 11 Tg/year based on the global marine N_2 fixation of 150 Tg/year and 1:1 molar stoichiometry (Brock & Madigan, 1991; Deutsch et al., 2007; Price et al., 2007). A spatially uniform loss rate constant for the surface ocean is assumed (Punshon et al., 2007) and gas transfer velocities estimated using the COAREG model modified for H_2 (Fairall et al., 2011; supporting information). Although surface ocean H_2 observations are sparse, this parameterization captures the basic latitudinal pattern of surface ocean saturation state, with supersaturation in warm waters and undersaturation at high latitudes (Herr et al., 1981, 1984; Scranton et al., 1982, 1984).

For the 2000 case, the box model yields a total tropospheric H_2 burden of 153 ± 26 Tg. The high-latitude Southern and Northern Hemispheres have H_2 levels of 545 ± 95 and 491 ± 81 ppb, in good agreement with modern flask air measurements and the South Pole firn air reconstruction (Novelli et al., 1999; NOAA/GMD: ftp://aftp.cmdl.noaa.gov/data/trace_gases/h2/).

To investigate whether the firn-air reconstruction is consistent with understanding of the modern budget, we developed a budget for 1910 from various literature sources. The 1910 budget was derived from the

modern budget by (1) reducing atmospheric methane levels to 881 ppb (Etheridge et al., 1998), (2) reducing anthropogenic emissions of H_2 to 10% of modern (Boden et al., 2016; supporting information), (3) reducing production from anthropogenic NMHC emissions to roughly 18% of modern (Lamarque et al., 2010), and (4) reducing emissions from terrestrial N_2 fixation by approximately half (Fowler et al., 2013). H_2 emissions from biogenic hydrocarbons and biomass burning were maintained at the same levels as in the 2000 simulation. Ocean H_2 production and partial atmospheric lifetimes for losses to soils, photochemistry, oceans, and stratosphere were assumed to be identical to those in the modern budget. In this simulation, the net sea to air H_2 flux increased by about 10% compared to the 2000 simulation, as a consequence of the increased air/sea H_2 difference. This budget has total H_2 sources of about 48 Tg/year.

The 1910 simulation gives a total atmospheric H_2 burden of 96 ± 20 Tg, and high-latitude Southern and Northern Hemisphere H_2 levels of 353 ± 76 ppb and 290 ± 61 ppb, respectively. The high southern latitude H_2 levels from the box model agree well with the firn air inversion result. To our knowledge, there is no published record of high northern latitude H_2 from this time period. Agreement between our estimated 1910 budget and the firn air reconstruction suggests that changes in anthropogenic emissions are likely responsible for most of the increase in 20th century atmospheric H_2. However, changes in the natural components of the budget are also possible and cannot be ruled out without additional constraints on the various budget terms.

The modeled atmospheric burden of H_2 increased by 37% over the 20th century, primarily driven by increasing anthropogenic emissions associated with fossil fuel burning and the anthropogenic increase in the atmospheric burden of methane. Because fossil fuel emissions are heavily biased toward the Northern Hemisphere, the modeled interpolar difference decreased from 63 ± 16 ppb in 1905 to 55 ± 21 ppb in 2000 ($p < 0.01$).

5. Conclusions

This study is the first Antarctic firn air reconstruction of the atmospheric history of H_2 for the 20th century. The results indicate that atmospheric H_2 levels over Antarctica increased from 357 ppb in 1910 to 548 ppb in 2000. These findings are consistent with the anthropogenic perturbation inferred from estimates of the modern inventory of atmospheric H_2 sources. Analysis using a simple biogeochemical model suggests that the global atmospheric H_2 burden increased over the 20th century by roughly 57 Tg (37%) and the N/S interpolar difference in H_2 decreased from about 63 to 55 ppb. Analysis of firn air at additional sites in both hemispheres is needed to validate these findings.

Data Availability Statement

The data used for this study are available at the U.S. Antarctic Program Data Center website (usap-dc.org; https://doi.org/10.15784/601332).

References

Aydin, M., Verhulst, K. R., Saltzman, E. S., Battle, M. O., Montzka, S. A., Blake, D. R., et al. (2011). Recent decreases in fossil-fuel emissions of ethane and methane derived from firn air. *Nature*, *476*(7359), 198–201. https://doi.org/10.1038/nature10352

Bader, H. (1964). Density of ice as a function of temperature and stress. *Special Report (U.S. Army Cold Regions Research and Engineering Laboratory)*, *64*, 1–6.

Bender, M. L., Sowers, T., Barnola, J. M., & Chapellaz, J. (1994). Changes in the O2/N 2 ratio of the atmosphere during. *Geophysical Research Letters*, *21*(3), 189–192. https://doi.org/10.1029/93GL03548

Boden, T. A., Marland, G., & Andres, R. J. (2016). Global, regional, and national fossil-fuel CO_2 emissions. Oak Ridge, TN. https://doi.org/10.3334/CDIAC/00001_V2016

Brock, T. D., & Madigan, M. T. (1991). *Biology of microorganisms* (6th ed.). EngleWood Cliffs, NJ: Prentice-Hall.

Butler, J. H. (1994). The potential role of the ocean in regulating atmospheric CH3Br. *Geophysical Research Letters*, *21*(3), 185–188. https://doi.org/10.1029/94GL00071

Craig, H., Horibe, Y., & Sowers, T. (1988). Gravitational separation of gases and isotopes in polar ice caps. *Science*, *242*(4886), 1675–1678. https://doi.org/10.1126/science.242.4886.1675

Deutsch, C., Sarmiento, J. L., Sigman, D. M., Gruber, N., & Dunne, J. P. (2007). Spatial coupling of nitrogen inputs and losses in the ocean. *Nature*, *445*(7124), 163–167. https://doi.org/10.1038/nature05392

Ehhalt, D. H., & Rohrer, F. (2009). The tropospheric cycle of H_2: A critical review. *Tellus Series B: Chemical and Physical Meteorology*, *61*(3), 500–535. https://doi.org/10.1111/j.1600-0889.2009.00416.x

Ehhalt, D. H., Schmidt, U., & Heidt, L. E. (1977). Vertical profiles of molecular hydrogen in the troposphere and stratosphere. *Journal of Geophysical Research*, *82*(37), 5907–5911. https://doi.org/10.1007/s11214-006-9067-0

Etheridge, D. M., Steele, L. P., Francey, R. J., & Langenfelds, R. L. (1998). Atmospheric methane between 1000 A.D. and present: Evidence of anthropogenic emissions and climatic variability. *Journal of Geophysical Research*, *103*(D13), 15,979–15,993. https://doi.org/10.1029/98JD00923

Fairall, C. W., Yang, M., Bariteau, L., Edson, J. B., Helmig, D., McGillis, W., et al. (2011). Implementation of the coupled ocean-atmosphere response experiment flux algorithm with CO_2, dimethyl sulfide, and O_3. *Journal of Geophysical Research*, *116*, C00F09. https://doi.org/10.1029/2010JC006884

Fowler, D., Coyle, M., Skiba, U., Sutton, M. A., Cape, J. N., Reis, S., et al. (2013). The global nitrogen cycle in the twenty-first century. *Philosophical Transactions of the Royal Society, B: Biological Sciences*, *368*(1621), 20130164. https://doi.org/10.1098/rstb.2013.0164

Herr, F. L., Frank, E. C., Leone, G. M., & Kennicutt, M. C. (1984). Diurnal variability of dissolved molecular hydrogen in the tropical South Atlantic Ocean. *Deep Sea Research Part A, Oceanographic Research Papers*, *31*(1), 13–20. https://doi.org/10.1016/0198-0149(84)90069-4

Herr, F. L., Scranton, M. I., & Barger, W. R. (1981). Dissolved hydrogen in the Norwegian Sea: Mesoscale surface variability and deep-water distribution. *Deep-Sea Research*, *28A*(9), 1001–1016.

Ikeda-Fukazawa, T., Fukumizu, K., Kawamura, K., Aoki, S., Nakazawa, T., & Hondoh, T. (2005). Effects of molecular diffusion on trapped gas composition in polar ice cores. *Earth and Planetary Science Letters*, *229*(3–4), 183–192. https://doi.org/10.1016/j.epsl.2004.11.011

Ildyakov, A. V., & Manakov, A. Y. (2014). Solubility of hydrogen in ice Ih at pressures up to 8 MPa. *International Journal of Hydrogen Energy*, *39*(33), 18,958–18,961. https://doi.org/10.1016/j.ijhydene.2014.09.069

Khalil, M. A. K., & Rasmussen, R. A. (1990). Global increase of atmospheric molecular hydrogen. *Nature*, *347*(6295), 743–745. https://doi.org/10.1038/347743a0

Lamarque, J. F., Bond, T. C., Eyring, V., Granier, C., Heil, A., Klimont, Z., et al. (2010). Historical (1850–2000) gridded anthropogenic and biomass burning emissions of reactive gases and aerosols: Methodology and application. *Atmospheric Chemistry and Physics*, *10*(15), 7017–7039. https://doi.org/10.5194/acp-10-7017-2010

Marik, T. (1998). *Atmospheric δ13C and δD measurements to balance the global methane budget, PhD thesis*. Heidelberg, Germany: Ruprecht-Karls-University.

Novelli, P. C., Lang, P. M., Masarie, K. A., Hurst, D. F., Mycrs, R., & Elkins, J. W. (1999). Molecular hydrogen in the troposphere: Global distribution and budget. *Journal of Geophysical Research*, *104*(D23), 30,427–30,444. https://doi.org/10.1029/1999JD900788

Paneth, F. A. (1937). The chemical composition of the atmosphere. *Quarterly Journal of the Royal Meteorological Society*, *63*(271), 433–443. https://doi.org/10.1002/qj.49706327114

Petrenko, V. V., Martinerie, P., Novelli, P., Etheridge, D. M., Levin, I., Wang, Z., et al. (2013). A 60 yr record of atmospheric carbon monoxide reconstructed from Greenland firn air. *Atmospheric Chemistry and Physics*, *13*(15), 7567–7585. https://doi.org/10.5194/acp-13-7567-2013

Pieterse, G., Krol, M. C., Batenburg, A. M., Steele, L. P., Krummel, P. B., Langenfelds, R. L., & Röckmann, T. (2011). Global modelling of H2 mixing ratios and isotopic compositions with the TM5 model. *Atmospheric Chemistry and Physics*, *11*(14), 7001–7026. https://doi.org/10.5194/acp-11-7001-2011

Prather, M. J. (2003). An environmental experiment with H_2. *Science*, *302*(5645), 581–582. https://doi.org/10.1126/science.1091060

Price, H., Jaeglé, L., Rice, A., Quay, P., Novelli, P. C., & Gammon, R. (2007). Global budget of molecular hydrogen and its deuterium content: Constraints from ground station, cruise, and aircraft observations. *Journal of Geophysical Research*, *112*, D22108. https://doi.org/10.1029/2006JD008152

Punshon, S., Moore, R. M., & Xie, H. (2007). Net loss rates and distribution of molecular hydrogen (H_2) in mid-latitude coastal waters. *Marine Chemistry*, *105*(1–2), 129–139. https://doi.org/10.1016/j.marchem.2007.01.009

Satoh, K., Uchida, T., Hondoh, T., & Mae, S. (1996). Diffusion coefficient and solubility measurements of noble gases in ice crystals. *Proceedings of the NIPR Symposium on Polar Meteorology and Glaciology*, *10*, 73–81.

Schmidt, U. (1974). Molecular hydrogen in the atmosphere. *Tellus*, *26*, 78–90. https://doi.org/10.1038/270297a0

Schultz, M. G., Diehl, T., Brasseur, G. P., & Zittel, W. (2003). Air pollution and climate-forcing impacts of a global hydrogen economy. *Science*, *302*(5645), 624–627. https://doi.org/10.1126/science.1089527

Schwander, J., Barnola, J. M., Andrie, C., Leuenberger, M., Ludin, A., Raynaud, D., & Stauffer, B. (1993). The age of the air in the firn and the ice at summit, Greenland. *Journal of Geophysical Research*, *98*(D2), 2831–2838. https://doi.org/10.1029/92JD02383

Scranton, M. I., Jones, M. M., & Herr, F. L. (1982). Distribution and variability of dissolved hydrogen in the Mediterranean Sea. *Journal of Marine Research*, *40*(3), 873–892.

Scranton, M. I., Novelli, P. C., & Loud, P. A. (1984). The distribution and cycling of hydrogen gas in the waters of two anoxic marine environments. *Limnology and Oceanography*, *29*(5), 993–1003. https://doi.org/10.4319/lo.1984.29.5.0993

Severinghaus, J. P., & Battle, M. O. (2006). Fractionation of gases in polar ice during bubble close-off: New constraints from firn air Ne, Kr and Xe observations. *Earth and Planetary Science Letters*, *244*(1-2), 474–500. https://doi.org/10.1016/j.epsl.2006.01.032

Tromp, T. K., Shia, R.-L., Allen, M., Eiler, J. M., & Yung, Y. L. (2003). Potential environmental impact of a hydrogen economy on the stratosphere. *Science*, *300*(5626), 1740–1742. https://doi.org/10.1126/science.1085169

Wang, D., Jia, W., Olsen, S. C., Wuebbles, D. J., Dubey, M. K., Rockett, A. A., & Wuebbles, C. D. J. (2013). Impact of a future H_2-based road transportation sector on the composition and chemistry of the atmosphere—Part 2: Stratospheric ozone. *Atmospheric Chemistry and Physics*, *13*, 6139–6150. https://doi.org/10.5194/acp-13-6139-2013

Wang, D., Jia, W., Olsen, S. C., Wuebbles, D. J., Dubey, M. K., & Rockett, A. A. (2013). Impact of a future H2-based road transportation sector on the composition and chemistry of the atmosphere – Part 1: Tropospheric composition and air quality. *Atmospheric Chemistry and Physics*, *13*(13), 6117–6137. https://doi.org/10.5194/acp-13-6117-2013